J. Phys. Chem. Solids, 1972, Vol. 33, pp. 2197–2216. Pergamon Press. Printed in Great Britain

ELECTRON TRAPPING LEVELS IN SILICON DIOXIDE THERMALLY GROWN ON SILICON*

J. H. THOMAS, III† and F. J. FEIGL
Materials Research Center and Department of Physics, Lehigh University, Bethlehem, Penna. 18015, U.S.A.

(*Received* 26 *August* 1971)

Abstract—Photocurrents associated with optical release of photoinjected electrons trapped in thin films of amorphous silicon dioxide have been studied. Temporal and spectral variation of the photocurrents were examined in detail: the effects on spectrally resolved response caused by variations in applied electrical field, wavelength sweep rate, and optical belaching are reported. All measurements were made on metal–oxide-semiconductor capacitors. The experiments were interpreted in terms of a straightforward model of optical excitation and transport of electrons out of localized energy levels in the silicon dioxide band gap. Semi-quantitative analysis indicated that a distribution of states peaked approximately 2·1 eV below the conduction band edge was associated with an electron trapping center distributed rather uniformly throughout the oxide film. In the wet thermal oxide specimens examined, the average density of trapping centers was greater than 10^{14} cm^{-3}. A time-stable spread in energy of approximately 0·5 eV was measured, and was attributed to local disorder in the amorphous insulator. The existence of an optically inactive charge distribution in the oxide films, with bulk average density greater than 10^{15} cm^{-3}, was indicated by collected charge vs. applied field data.

1. INTRODUCTION

RECENTLY there has been intense interest in the defect structure of thin films of silicon dioxide due to their extensive use as passivating and insulating layers in the silicon planar technology [1, 2]. Interface charges and states, at or near oxide–metal and oxide-semiconductor boundaries, are of major importance in device and integrated circuit performance. Interface states of primary interest are associated with electron or hole levels lying energetically in the semiconductor forbidden gap, and may be associated with impurities, structural defects, or general disorder in the vicinity of the semiconductor-oxide interface [3, 4].

Interface phenomena in metal–oxide-semiconductor (MOS) structures have been studied in great detail using electrical techniques—primarily capacitance and differential conductance measurements [5–10]. These techniques are most sensitive to charge variations at the semiconductor-oxide interface. Photoemission measurements [11–17] have been used to determine the energy band diagram for the MOS structure (particularly interface barrier heights in metal–silicon dioxide–silicon systems) and to study electronic injection into the silicon dioxide film [11, 12, 18–22].

Structural defects and impurities in the bulk of the insulator may produce energy levels lying in the forbidden gap of the insulator. These states may constitute trapping levels for electrons or holes. Charge trapped at these sites can affect both the electrical and optical properties of the insulator, and may affect the properties and performance of the device in which it is incorporated. There has been some interest in the relation between impurity and defect centers in the oxide bulk and the defect structure at the interfaces [23–25], and considerable speculation exists on the role played by oxide impurities and defects

*Research supported in part by U.S. Navy Office of Naval Research, contract N00014-67A-0370. Based in part on a dissertation submitted by J. H. Thomas, III, to Lehigh University in partial fulfillment of the requirements for the Ph.D. degree.

†National Science Foundation Trainee and General Telephone and Electronics Pre-Doctoral Fellow. Present Address: Bell Telephone Laboratories, 6200 East Broad Street, Columbus, Ohio 43213, U.S.A.

in degradation of device performance by ambient radiation [26–30].

The deep trapping states associated with the insulator bulk can also be studied by the optical or electrical measurement techniques mentioned above. Both capacitance and conductance techniques have been used to study fixed charge [31] and mobile charge migration [32] in the silicon dioxide layer of an MOS structure. Photoemission techniques have also been used to examine the role of trapping phenomena in controlling electronic transport into and across thermally grown oxide films [11, 12, 18–22]. The recent detailed studies of Powell indicated that trapping effects are negligible in thin films [20, 22]. This differs from the earlier interpretation of Williams and Goodman for thick films [11, 12, 17].

In a recent communication the present authors presented the results of a study on defect-related electronic properties of thin films of silica incorporated in an MOS structure [33]. The characteristics of an electronic state distribution apparently associated with an electron trapping defect in silicon dioxide produced by steam oxidation of silicon were reported. The observed photoconductive response was associated with a relatively symmetric inhomogeneously broadened state distribution, approximately 0·5 eV wide and centered approximately 2·1 eV below the conduction band edge in silicon dioxide. The maximum concentration of the charged defects in the samples studied was typically 10^{14} cm^{-3} (bulk average), in agreement with that reported by Williams [11].

The present paper presents a detailed description of the measurements described in the communication [33]. In addition, several previously unreported experiments, independently supporting the conclusions of the communication, are described and analyzed in detail.

2. EXPERIMENTAL DETAILS

Specimen preparation and experimental techniques and equipment used in the present investigation are as described in the communication [33]. MOS devices were used in all measurements. The samples were steam grown oxides on degenerate *n*-type silicon substrates (⟨111⟩ orientation, resistivity of order 10^{-2} Ω-cm) obtained from two different sources (see Table 1).* Oxide thickness ranged from 1 to 4 μm. The oxide thickness was determined by measurement of the wavelengths of interference fringes in normal reflectance spectra. The measurements agreed closely with thickness determinations via interference effects in photocurrent spectra, described by Goodman [12, 34].

Table 1. Thermal oxide specimens used in the present investigation. All specimens were fabricated by a steam–air oxidation process on ⟨111⟩ orientation degenerate n-type silicon substrates. Substrate resistivities were 0·005–0·015 Ωcm

Sample number	Source	Oxide thickness
1	RCA–Princeton	4·0 μm
2	Bell–Murray Hill	2·5 μm
3	Bell–Murray Hill	4·2 μm

Semi-transparent gold films vacuum evaporated on the silicon dioxide layer were used as the metal electrode of the MOS capacitor (to allow illumination of the oxide in the presence of an external applied field). The semi-transparent electrodes were typically 2 mm × 10 mm × 10^{-2} μm thick. The thickness of the semi-transparent electrodes was determined by comparative transmittivity measurements at 800 nm, using a Beckman i.r. spectrophotometer [34]. The transparent electrodes were in contact with a 2 mm dia. × 1 μm thick vapor deposited gold dot for probe contact, and the clean back surface of the silicon substrate was provided with a vapor deposited 1 μm thick

*Samples used in the present investigation were obtained through the generosity of Dr. Richard Powell of Bell Telephone Laboratories, Murray Hill, and Dr. Alvin Goodman of the RCA Laboratories, Princeton.

gold overlayer to insure noise-free contact to the external circuitry.

The basic instrumentation used in the experimental program is illustrated in Fig. 1. It consists of a light source (either an u.v. source consisting of the unfiltered output of a 60 W deuterium lamp limited by silica optics, or the monochromatic visible source illustrated in Fig. 2), a specimen chamber, and the external circuit electronics. The electronic circuitry consisted of a variable voltage supply

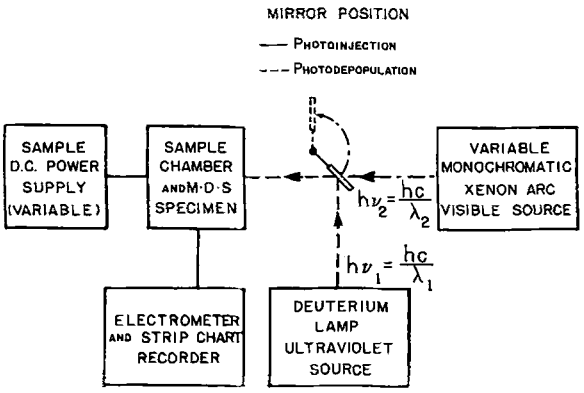

Fig. 1. Block diagram of experimental system used for photoinjection and photodepopulation measurements. As indicated in the diagram, the front surface mirror was used to select u.v. radiation (wavelength λ_1, for photoinjection) or visible radiation (wavelength λ_2, for photodepopulation).

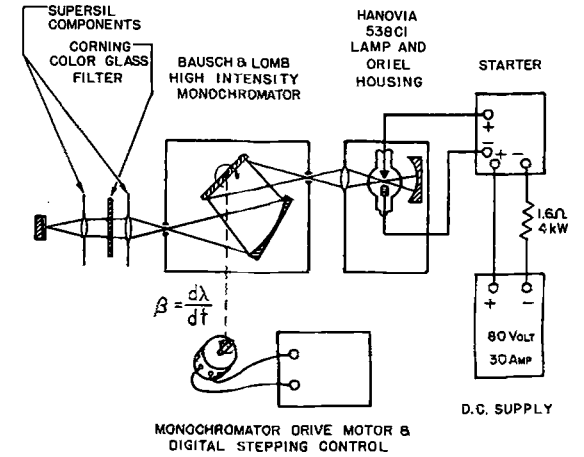

Fig. 2. Schematic representation of the optical system used for photodepopulation measurements.

(batteries and a potentiometer), a Keithley model 600 A battery-operated electrometer, and a variable speed strip chart recorder.

A cylindrical specimen chamber was outfitted with large vacuum flanges at both ends. A supersil window in one of the end flanges, and several sideport electrical and gas valve connections, were vacuum sealed. The specimen was mounted on either of two brass blocks in a vertical plane by a pressure front contact. For room temperature measurements, a brass block was mounted on a thick teflon slab attached to the interior of the end flange opposite the optical window. For measurements between 80 K and room temperature, the brass sample mounting block constituted the cold finger of a quarter-liter capacity glass liquid nitrogen dewar. The cold finger of the dewar was inserted into the chamber through a standard vacuum feedthrough. Teflon was used to insulate all electrical and mechanical contacts to the specimen mounting block and front contact probe. The specimen could be examined in various ambients—vacuums below 10^{-5} torr, inert gases, or dry air (using dessicants).

The basic experiments executed in the course of this investigation can be described in terms of the very schematic energy level diagrams in Fig. 3. As indicated by Figs. 1–3, the important variables in all the experiments are (1) applied voltage across the MOS capacitor (sign and magnitude) and (2) illumination conditions (intensity and spectral distribution). The variable which was measured was the current in the external circuit. This was generally interpreted as a photocurrent. A given experiment consisted of two steps—*photoinjection* of charge carriers into the silicon dioxide, and *photodepopulation* of the filled trapping levels, under controlled conditions, producing photocurrent in the external circuit. These processes are discussed separately below.

(a) *Photoinjection*

Defects and impurities in a solid can act as

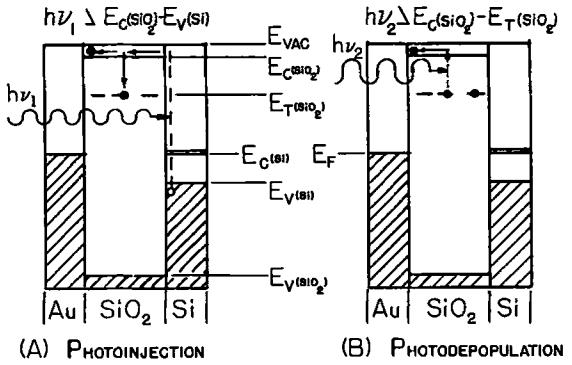

Fig. 3. Idealized energy band diagram of (a) the photoinjection process and (b) the photodepopulation process. In both cases, the semi-transparent gold electrode is biased positive with respect to the silicon substrate. Electron transport is thus from Si to Au, as indicated. $h\nu_1$ and $h\nu_2$ are the incident photoenergies during photoinjection and photodepopulation, respectively. The subscripts C, V and T indicate conduction band edge, valence band edge, and inter-band trapping level, respectively. E_F is the Fermi level and E_{VAC} the vacuum level.

electron and hole trapping centers, since the electronic states associated with these centers may be relatively well localized and be associated with one-electron energies within the forbidden gap of the insulator[35–38]. In the present experiment, electrons are introduced into the silicon dioxide conduction band by photoemission from the optical surface of the silicon electrode. Photon energies $h\nu_1$ greater than the Si–SiO_2 barrier height $E_B = E_C(SiO_2) - E_V(Si)$ are required (See Fig. 3(a)), and the photoemission and transport across the oxide are most efficient in the presence of relatively high accelerating fields. Some fraction of the electrons introduced into the insulator conduction band are captured into stable deep traps, at energy E_T (Fig. 3(a)). This technique for obtaining measurable concentrations of charged traps (populated deep trapping levels) is referred to as *photoinjection*.

Previous investigations have shown that the photoinjection process involves essentially electronic rather than hole injection into the insulating layer of the MOS sandwich[11, 12, 18]. The basic photoemission experiments of Williams[11] and Goodman[12] were repeated in connection with the present research. For the specimens used, the threshold for strong photoemission occurred at photon energies of approximately 4·2 eV ($E_C(SiO_2) - E_V(Si)$), with a long wavelength tail due to weak photoemission exhibiting a threshold of approximately 3·1 eV ($E_C(SiO_2) - E_C(Si)$)[12, 14, 19].

Utilizing the full output of the u.v. source described above, and applied fields of approximately 5×10^5 V/cm, photoemission currents of order 10^{-9} A were observed. These conditions produced stationary bulk average trap concentrations of order 10^{14} cm^{-3} in times of 30 min[11]. These 'standard fill conditions' were used throughout the program of measurements, except as specifically noted.

(b) *Photodepopulation*

The photoinjection technique just described permits the electronic properties of charged defects to be studied without the usual complication of irradiating the material with ionizing photons or particles[39]. Detailed information on the electronic structure of the charged defects obtained by photoinjection can be in principle obtained by optically stimulated trap emptying, as described by Bube[40]. This, basically, is the technique used in the present study – photodepopulation.

Traps filled by photoinjection of charge are optically active, that is, they can be emptied by photons of the proper energy $h\nu_2 > E_C(SiO_2) - E_T(SiO_2)$ (see Fig. 3(b)). Depopulation of the trapping centers was accomplished by illuminating a trap filled sample, subject to high electric fields, with the high intensity monochromatic source described above (Fig. 2). Electrons trapped in defect centers were thus excited to the conduction band of the silicon dioxide (Fig. 3(b)). Under the influence of the applied field, the photoexcited electrons were swept out of the oxide to one of the two electrodes. Current due to the transport of optically excited electrons was recorded as a function of time and wavelength of incident illumination in the external circuit. Experiments performed can be

classified as time resolved and spectrally resolved measurements.

Time resolved photodepopulation. If an MOS specimen charged by photoinjection is illuminated by monochromatic radiation of frequency ν_2, all traps with energy $E_C(SiO_2) - E_T(SiO_2)$ less than $h\nu_2$ can be emptied and the resultant charge collected on one of the sample electrodes. This assumes that no retrapping or recombination occurs within the oxide. The external circuit photocurrent, recorded as a function of time under constant illumination conditions and fixed voltage, is denoted *time resolved photodepopulation.* Results of time resolved photodepopulation experiments are exhibited in Fig. 4. The variable parameter for the several curves is the voltage applied across the MOS capacitor.

Spectrally resolved photodepopulation. As indicated in Fig. 2, the monochromatic visible light source used in photodepopulation experiments was designed so that the illumination wavelength could be driven at a constant rate $\beta = d\lambda/dt$ (measured in nm/sec). Photoinjected charge can thus be released while sweeping the monochromator from long to short wavelengths at a constant rate. The external circuit current, recorded as a function of time, can then be interpreted as a spectral resolution of the photocurrent (photocurrent vs. wavelength), using the relation $\lambda = \lambda_0 + \beta t$. Here λ_0 is the starting wavelength. This measurement is denoted *spectrally resolved photodepopulation.* Figure 5 exhibits spectrally resolved photodepopulation data typical of most specimens examined during the present experimental program. This is the raw data from which the experimental points of

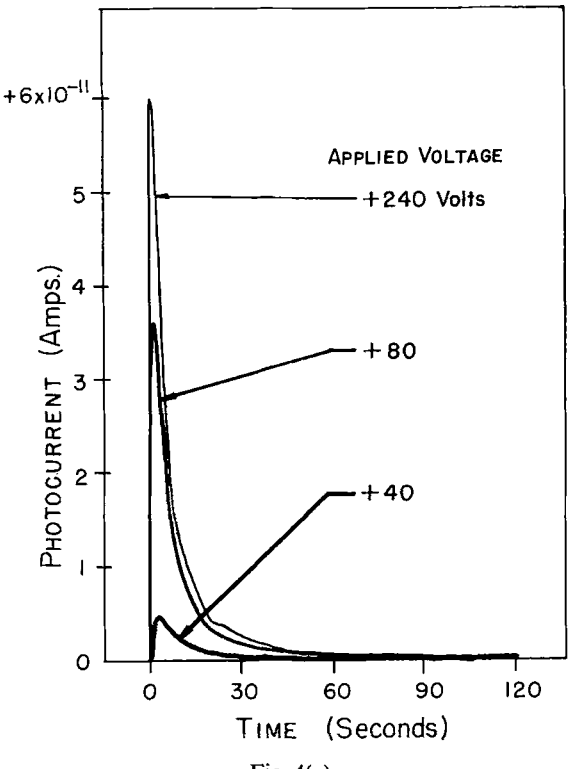

Fig. 4(a)

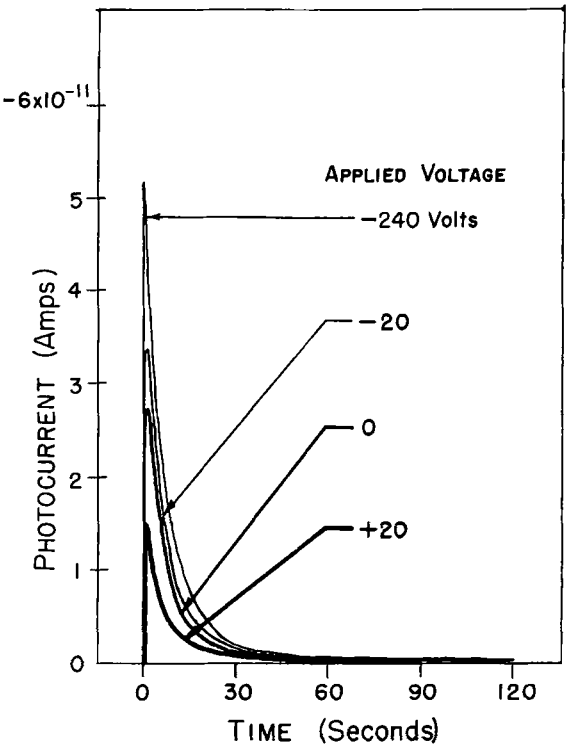

Fig. 4(b)

Fig. 4. Time resolved photodepopulation response for sample number 1. Electrode area 0·18 cm². Positive polarity refers to gold electrode biased positive with respect to silicon substrate. (a) positive photocurrent (net electron transfer from silica to gold), (b) negative photocurrent (net electron transfer from silica to silicon). Monochromator setting $\lambda_2 = 450$ nm, band pass 20 nm.

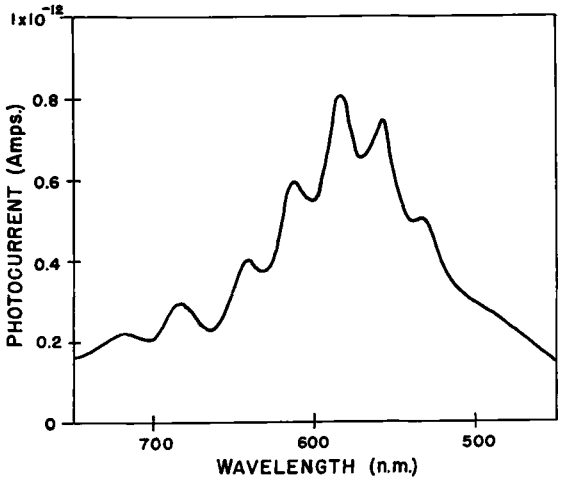

Fig. 5. Spectrally resolved photodepopulation data for sample number 1. Electrode area 0·18 cm². Monochromator sweep rate, β, was 0·3 nm/sec. This is a strip chart recorder tracing, with noise fluctuations smoothed.

Fig. 2 of Thomas and Feigl [33] were obtained. Undulations in the data are due to thin film interference effects, as described in the earlier communication [33]. These effects are analyzed in the Appendix to the present paper.

3. EXPERIMENTAL RESULTS

(a) *Time resolved measurements*

Time resolved photodepopulation measurements, as described in Section 2(b), have been performed with applied voltage varied as a parameter. Traps were populated according to the set of 'standard fill conditions' described in Section 2(a). The monochromatic depopulation source was set at 450 nm, with a 20 nm band pass. Photodepopulation current at a given applied field was recorded on the strip chart recorder, and is indicated in the insets on Fig. 6. The time resolved photodepopulation data were mechanically integrated, and total collected charge was plotted as a function of the applied field. These are the data points exhibited in Fig. 6.

As indicated in Fig. 11, applied fields in the oxide were defined as positive for electron acceleration towards the metal electrode, and current was defined as positive for electron

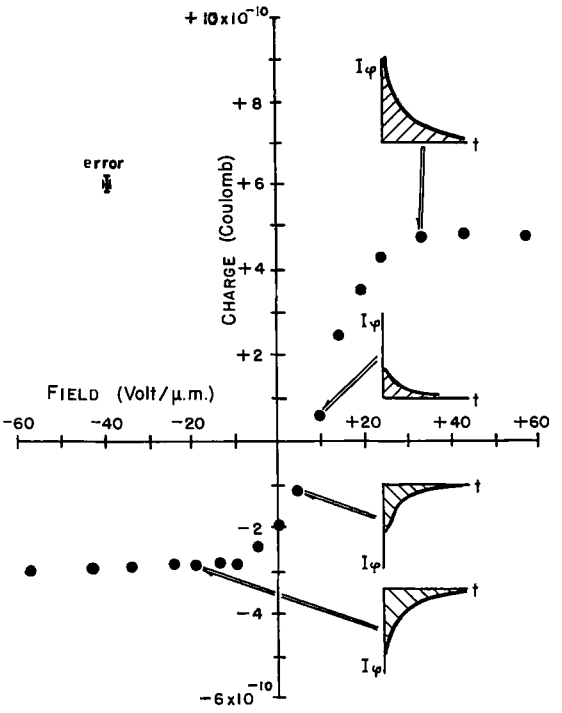

Fig. 6. Charge collected as a function of applied field during photodepopulation. Sample number 1, electrode area 0·18 cm². Positive voltage refers to gold electrode biased positive with respect to silicon substrate; positive charge refers to net electron transfer from silica to gold. The insets ($I\varphi$ vs. t) represent time resolved responses from which data points were calculated.

currents in the external circuit from the metal electrode to the silicon electrode. A net positive collected charge thus corresponded to a net negative charge collected at the metal electrode (i.e., a net *electron* transport from the insulator to the metal electrode).

The important features of the data shown in Fig. 6 can be summarized as follows:

1. For large positive and negative applied fields, the charge collected tended towards a saturation value—the positive and negative saturation charges were not equal;
2. For zero applied field, a negative photocurrent was observed, corresponding to a net negative charge collected on the silicon electrode; and
3. At some positive applied field, the net charged collected was zero.

(b) *Spectrally resolved measurements*

Spectrally resolved data were obtained after traps had been populated according to the set of 'standard fill conditions' described in Section 2(a). The following depopulation parameters were varied and their effects on the spectrally resolved photocurrent response studied in detail: (1) depopulation voltage; and (2) monochromator sweep rate.

Depopulation voltage variations. Photocurrent responses exhibited in Fig. 7 were obtained for different applied voltages during depopulation. Throughout this series of measurements, illumination conditions were held constant: monochromator passband of 20 nm, monochromator sweep rate of 0·3 nm/sec (refer to Section (2b) and Fig. 2).

There are two important features of the data of Fig. 7. First, the shape of the spectrally resolved photocurrent response did not vary significantly with applied field, and second, the amplitude of the spectrally resolved photocurrent response was a strong function of applied field. By changing the wavelength axis of the data to time and integrating these data to find total charge released, the charge vs. applied field data of Fig. 6 were reproduced within the error of the measurements.

Sweep rate variations. The spectrally resolved photocurrent response was observed to vary with sweep rate, as described in

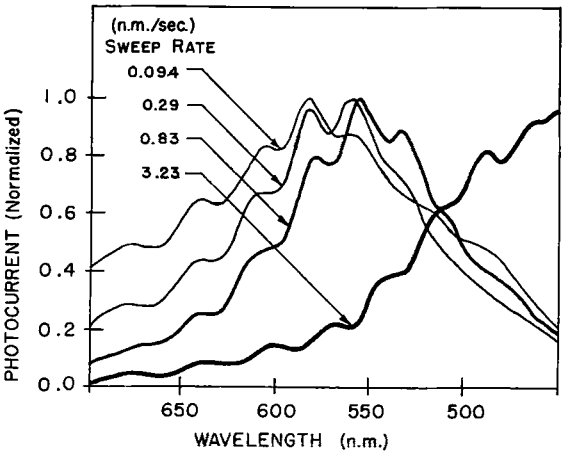

Fig. 8. Spectrally resolved photodepopulation response for various monochromator sweep rates. Monochromator band pass 20 nm/ sec. Sample number 1. Photocurrent is shown normalized to maximum value.

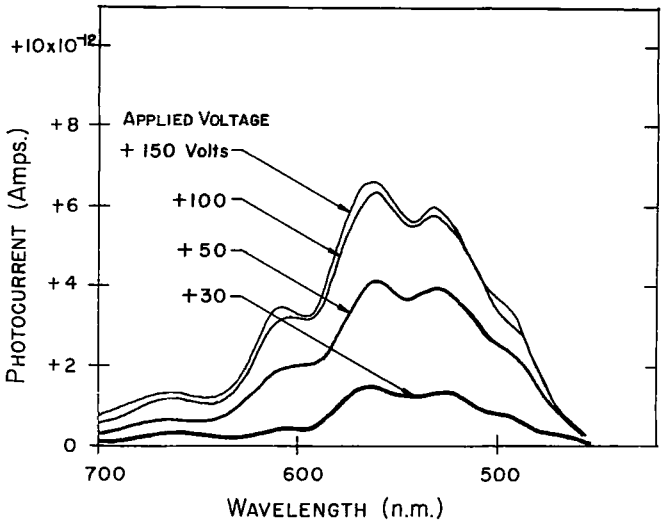

Fig. 7. Spectrally resolved photodepopulation response for various applied voltages. Sample number 2, electrode area 0·18 cm². Monochromator sweep rate 0·2 nm/sec, band pass 20 nm. Positive voltage refers to gold electrode biased positive with respect to silicon substrate.

Thomas and Feigl[33]. Figure 8 shows photocurrent response for selected sweep rates ($\beta = d\lambda/dt$, in nm/second—refer to Section 2(b) and Fig. 2). Fill conditions and depopulation voltage were constant—voltages were set in the positive saturation region of Fig. 6. Data shown were normalized to maxima in order to emphasize the strong variation of the shape of the spectrally resolved photocurrent response with sweep rate. In general, the response peak position shifted to shorter wavelengths with increasing sweep rate. The variation was largest at the largest sweep rates, and the normalized response curve became stationary at the smallest sweep rates. Photocurrent response amplitude was observed to decrease with decreasing sweep rate. The total amount of charge released by sweeping from 700 to 450 nm was constant, except at the fastest sweep rate.

(c) *Optical bleaching measurements*

The effect of optical bleaching on the photocurrent response has been studied. Traps in the insulating film were again populated according to standard fill conditions (Section 2(a)). A time-resolved photodepopulation measurement was then performed, with the monochromator set at wavelength λ_b for a period of 20 min. Subsequent to this, spectrally resolved photocurrent response was measured from 700 to 450 nm at a sweep rate of 0·3 nm/sec. This sequence was repeated for a number of different bleaching wavelengths λ_b. The spectrally resolved photocurrent data $I_{\lambda_b}(\lambda)$ is exhibited in Fig. 9. Data for each bleaching wavelength were then normalized to the i.r.-bleached data ($I_{750}(\lambda) \equiv I_{\text{i.r.}}(\lambda)$), and 'bleaching profiles' were plotted, as indicated in Fig. 10.

The bleached photocurrent response (Fig. 9) and the bleaching profiles (Fig. 10) indicated that the portion of the spectrally resolved photocurrent response with wavelength $\lambda > \lambda_b$ has been eliminated by the bleaching treatment (i.e., by illumination at wavelength λ_b). In general, some reduction of photocurrent response across the entire range of wavelengths was observed (Fig. 10). Bleaching at $\lambda_b = 450$ nm completely eliminated the

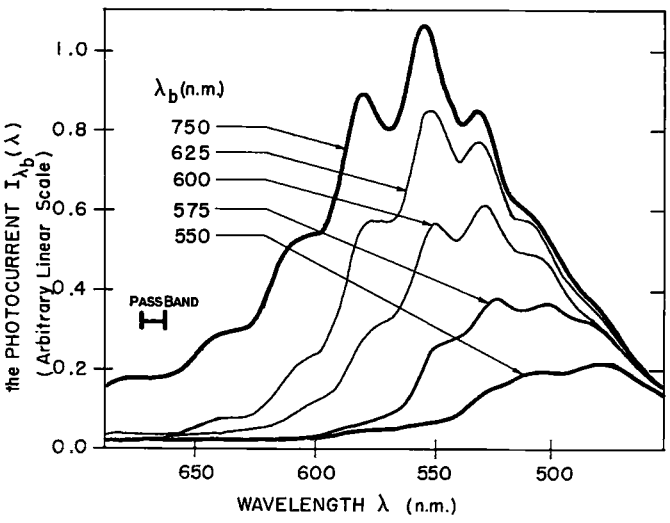

Fig. 9. Spectrally resolved photodepopulation response subsequent to a twenty-minute optical bleach at the indicated wavelength λ_b, using a 10 nm monochromator band pass. as indicated. Sample number 1. Spectrally resolved data obtained with monochromator sweep rate 0·3 nm/sec, and monochromator band pass 20 nm.

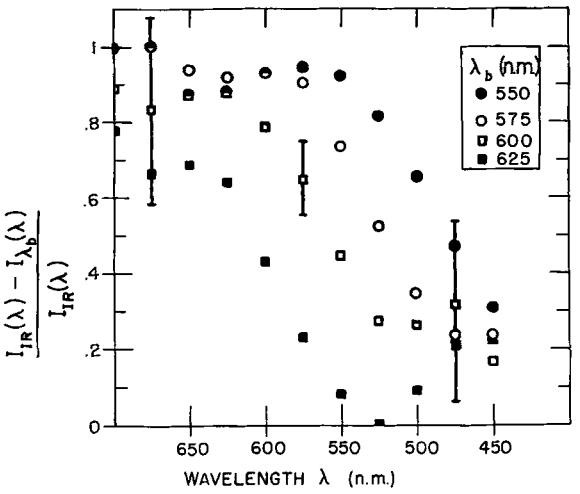

Fig. 10. Bleaching profiles. Bleached spectrally resolved photodepopulation responses (Fig. 9) were normalized as indicated to the 750 nm bleached spectrally resolved response $I_{i.r.}(\lambda)$.

spectrally resolved photocurrent response. One important feature of this data was that the *shape* of the bleaching profiles (Fig. 10) was not a strong function of the bleaching wavelength λ_b.

4. ANALYSIS

Implicit in the conclusions of the Thomas and Feigl communication[33], and in the description of experiments in Sections 2 and 3, was a particular and relatively detailed model of the optically stimulated trap emptying process in thermal silica films. In this section, the assumptions and approximations of this model are stated, the results of analytical solutions of the model problem are presented, and the results of a numerical analysis of the experiments within the framework of the model problem are given. The three major results of Section 3 are analyzed separately (the collected charge vs. applied field data of Figs. 6 and 7, the variable sweep rate measurements of Fig. 8, and the bleaching profile of Fig. 10.) Emphasis is on a comprehensive qualitative description. A complete critical discussion of the overall logic will be presented elsewhere.

The analysis of the photodepopulation experiments began with the presumed results of the photoinjection process (Section 2(a)): the existence, throughout the bulk of the insulating film, of a distribution of trapped electronic (negative) charge $n_T\rho(x,\epsilon)=n_T\rho'(x)\rho''(\epsilon)$, where x is the depth from the metal–oxide interface and ϵ is the energy separation of the trapping level from the conduction band edge, E_C-E. The injected trapped charge distribution was presumed homogeneous in the plane of the film, so that the only spatial variation of concern was along the x-direction, perpendicular to the plane of the film. No presumption was made regarding the nature of the trapping sites (i.e., whether they were neutral before or after trapping the electrons), so the *net* charge of the insulator was not specified. In order to avoid complications not relevant to the present experiments, the charge distribution $n_T\rho(x,\epsilon)$ existing after a standard fill was explicitly assumed to represent a situation in which all available electron trapping centers of a given type are charged (i.e., have trapped an electron)*.

A further assumption had to be made concerning the distribution of charge within the insulating layer. It was assumed that there was a charge distribution $N_TP(x)$ distributed throughout the insulator film. This charge distribution, which was designated as the *fixed* charge to distinguish it from the *injected* $n_T\rho(x,\epsilon)$, was also presumed to be homogeneously distributed in the y and z directions (the plane of the film). The distribution $N_TP(x)$ represented any deviation from neutrality on a microscopic or macroscopic scale not associated with the injected trapped charge $n_T\rho(x,\epsilon)$. For simplicity, $N_TP(x)$ was presumed homogeneous in sign throughout the film. $N_TP(x)$ was presumed to be invariant throughout the photoinjection–photodepopulation process described in Section 2.

*This assumption, although critical in regard to the current very active dispute interest concerning transport and current injection in MOS structures, was made here for convenience only. The present experiments did not allow a critical statement to be made on this point. Further comments shall be made in Section 5.

Figure 11 presents a summary of the model used for the M–O–S structure. Both electrodes (the silicon substrate and the semitransparent gold electrode) were treated as low resistivity contacts. Again, this assumption was made for convenience since the present experiments did not critically test the interface situation. The electrode properties only entered the determination of the optical intensity within the oxide film, as discussed in the Appendix.

The three major experiments described in Section 3 will be separately analyzed within the framework of the model summarized in Fig. 11. In each case, a simplified model for optical excitation and electronic transport within the insulator was used, together with a specification of the injected charge distribution $\rho(x, \epsilon)$ appropriate to the experiment.

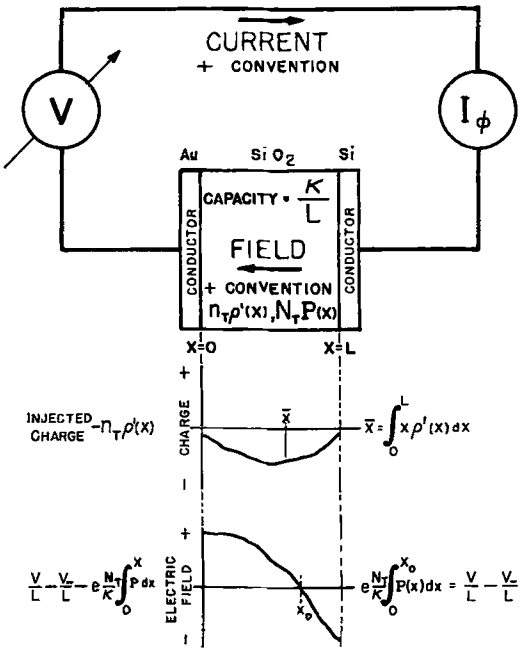

Fig. 11. Schematic representation of MOS capacitor model employed in analyzing data. κ is the static dielectric constant of bulk amorphous silica. Field and current conventions are as indicated. A representative injected charge distribution $n_T\rho'(x)$ and internal fields associated with a representative fixed charge distribution $N_T P(x)$ are indicated in the diagram. $I\varphi$ is the photocurrent, and V, the applied field, must be corrected for the difference between the gold work function and the silicon electron affinity.

(a) *Collected charge vs. applied field measurements*

In analyzing the time resolved photodepopulation measurements, it was assumed that the quantum energy of visible radiation ($h\nu_2$ of Fig. 3) was greater than the trap depth $\epsilon = E_C(SiO_2) - E$ of any of the states in the distribution $\rho(\epsilon, x)$. Further it was assumed that all traps were emptied at a uniform rate proportional to the photon density. Once excited into the conduction band, released electrons drifted to one or the other electrode, without retrapping, under the influence of the internal fields arising from resultant of the fixed charge distribution $N_T P(x)$ and the applied voltage V.

The simplest statement of this complex of approximations is depicted schematically in Fig. 12. In terms of the distribution described above, it was assumed that

$$n_T\rho(x, \epsilon) = n_T\delta(\epsilon - \epsilon_T)\rho'(x) \qquad \text{and} \quad n_T \ll N_T$$

where

$$\int_0^L \rho'(x)\,dx = \int_0^L P(x)\,dx = 1.$$

Throughout the photodepopulation process the density of filled traps was assumed to vary according to $n_T(t) = \exp(-\alpha t)$, with α proportional to photon density. Thus, n_T and N_T are the total amount of injected and fixed charge per unit area, respectively.

The problem reduces to an ideal parallel plate capacitor analysis, with the result that

$$\frac{dq(V/L)}{d(V/L)} = -\kappa\frac{\rho'(x_0[V/L])}{P(x_0[V/L])}$$

for applied fields below saturation (refer to Fig. 4). Here, κ is the static dielectric constant of the oxide (presumed equal to the bulk value), q is the net charge collected from released carriers and $x_0[V/L]$ is the zero field

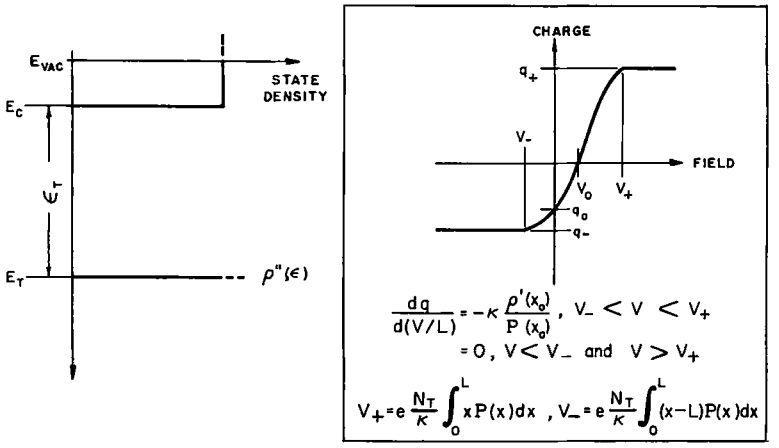

Fig. 12. Schematic representation of electronic structure model for SiO_2 used in analyzing time resolved photodepopulation data. For photon energy $h\nu_2 > \epsilon_T$, electrons are excited from the trap level at ϵ_T to the conduction band. The inset at right contains a synopsis of results to be expected in collected charge vs. applied voltage experiments.

position in the insulator at an applied field V/L (see Fig. 11). The collected charge saturated (i.e., $dq/d(V/L) = 0$) for positive (negative) applied fields exceeding the maximum negative (positive) internal fields associated with the fixed charge $N_T P(x)$. The positive and negative saturation charges were designated $q+$ and $q-$, respectively.

In principle, the spatial distribution of both the fixed and injected charges could be determined from the charge vs. applied field curve if an independent determination of either one could be made. In practice, only the ratio has been determined. However, four important characteristics of the relevant spatial distribution were specified:

(1) The average density (number per cm^3) of filled traps

$$\frac{n_T}{L} = \frac{q_+ + |q_-|}{eL}$$

where e is the electronic charge,

(2) The centroid of the filled trap distribution

$$\bar{x} = \int_0^L x\rho'(x)\,dx = \frac{q_+ L}{q_+ + |q_-|}$$

(3) The average density of fixed charges

$$\frac{N_T}{L} = \frac{\kappa}{eL^2}(V_+ + |V_-|),$$

(4) The centroid of fixed charge

$$\bar{X} = \frac{V_+ L}{V_+ + |V_-|}.$$

A summary of the analysis just described is also illustrated in Fig. 12. A tabular summary of results obtained from the data of Fig. 6 is given in Table 2.

(b) *Variable sweep rate measurements*

In analyzing the spectrally resolved photodepopulation experiments, the ideal capacitor model for the MOS structure was assumed (Section 4(a)). In addition, a specific model for an extended distribution of trapping states $\rho''(\epsilon)$ was assumed. It was again assumed that traps were emptied into the conduction band at a rate proportional to the photon density, but that only traps with energy relative to the conduction band edge *less than* $h\nu_2$, the quantum energy of the excitation source, were excited.

Table 2. Characteristics of injected and fixed charge distributions. The centroid of the injected charge distribution was determined to be independent of the voltage applied during photoinjection

Injected charge distribution
$\frac{n_T}{L} = (0{\cdot}60 \pm 0{\cdot}05) \times 10^{14}\ \text{cm}^{-3}$
$\frac{\bar{x}}{L} = 0{\cdot}62 \pm 0{\cdot}05$
Fixed charge distribution
$\frac{N_T}{L} = (2{\cdot}6 \pm 0{\cdot}3) \times 10^{15}\ \text{cm}^{-3}$
$\frac{\bar{X}}{L} = 0{\cdot}70 \pm 0{\cdot}05$

The model of the electronic structure of the insulating film employed is illustrated in Fig. 13. This is a plot of density of states vs. energy and illustrates a step function approximation to the conduction band and a trapping state distribution approximated as a semi-continuous distribution of discrete (δ-function) levels. The distribution envelope was assumed gaussian for convenience, and constituted an ideal inhomogeneous distribution of trapping levels [41]. This is consistent with the assumption that the trapping level distribution was associated with a given type of defect structure and that the time-stable 'spread' in energy was associated with local disorder in the amorphous insulating layer. In the spectrally resolved photodepopulation measurements, the wavelength of the excitation light was varied continuously and linearly with time from the low to high energy end of the electronic state distribution, and the external circuit current resulting from trap emptying was continuously monitored. The data was plotted as photocurrent (assumed directly proportional to the trap release rate) vs. wavelength, using time as an intermediate parameter (see Section 2(b) and Fig. 8).

In terms of the distributions listed above, the simplest mathematical form for the injected charge distribution is

$$n_T \rho(x, \epsilon) = n_T \delta(x - \bar{x}) \quad \frac{1}{\sqrt{2\pi}\,\delta} e^{-\frac{(\epsilon - \epsilon_T)^2}{2\delta^2}}$$

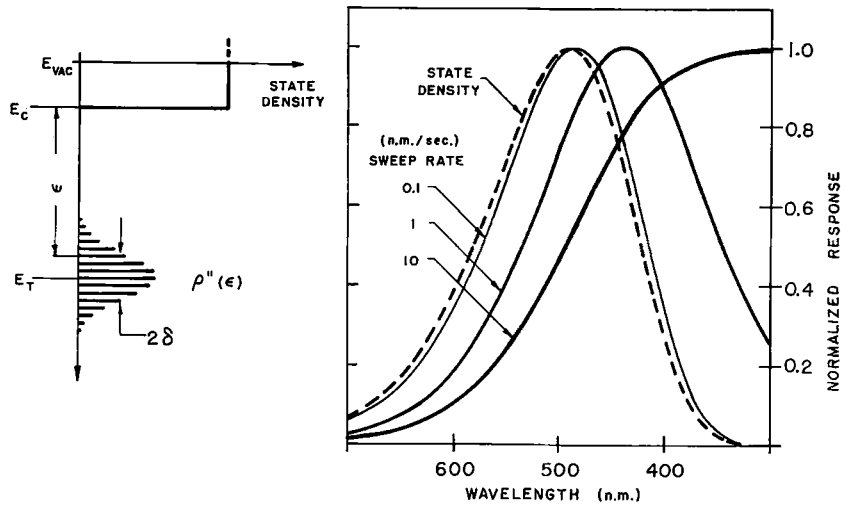

Fig. 13. Schematic representation of electronic structure model for SiO_2 used in analyzing variable sweep rate spectrally resolved photodepopulation data. For photon energy $h\nu_2$, all electrons in trap levels of energies $\epsilon < h\nu_2$ are excited to the conduction band. The inset at right contains representative results to be expected in variable sweep-rate experiments.

where ϵ_T, the trap depth, is the energy of the peak of the trap level distribution and δ is the width, in energy, of the distribution. As in Section 4(a), $\bar{x}$ is the centroid of the actual spatial distribution:

$$\bar{x} = \int_0^L x\rho'(x)\,dx.$$

If α is defined as the transition rate for excitation (proportional to the light intensity in the film) and $\beta = d\lambda/dt$ as the sweep rate (nm/sec.) of the excitation source, it can be shown that the photocurrent response function $R(\lambda)$ is given by

$$\frac{1}{\alpha}\frac{dR(\lambda)}{d\lambda} + \frac{1}{\beta}R(\lambda) = n_T\rho''(\lambda)$$

where $\rho''(\lambda)$ is the distribution of trapping states in wavelength corresponding to the presumed distribution in energy

$$\rho''(\epsilon) = \frac{1}{\sqrt{2\pi}\delta}e^{-\frac{(\epsilon-\epsilon_T)^2}{2\delta^2}}$$

In the above expressions, $\epsilon = h\nu_2 = (hc/\lambda_2)$.

In the limit of very slow sweep rate ($\alpha/\beta \gg 1$), $R(\lambda) = \beta n_T\rho''(\lambda)$ and the observed response function was directly related to the energy distribution function of the trapping levels. In the limit of very fast sweeprate ($\alpha/\beta \ll 1$), $dR(\lambda)/d\lambda = \alpha n_T\rho''(\lambda)$ so that the response function was proportional to the integral of the trap distribution function

$$R(\lambda) \propto \int_{-\infty}^{\lambda} \rho''(\lambda')\,d\lambda'.$$

The results of a model calculation, using this analysis, are also shown in Fig. 13, in which the response function is exhibited at several sweep rates. This is to be compared with the experimental results exhibited in Fig. 8. The experimental peak position at different sweep rates, determined by a graphical technique, was compared with computed peak positions. This permitted extrapolation to a 'zero sweep rate' peak position, the 'true' position (ϵ_T) of the trapping level distribution. These results are exhibited in Fig. 14. In analyzing this data, the transition rate α was as adjustable parameter. The value of α obtained from fitting this data agreed satisfactorily with the decay time observed in the time resolved experiments (Fig. 3), within the overall limits of precision of the data.

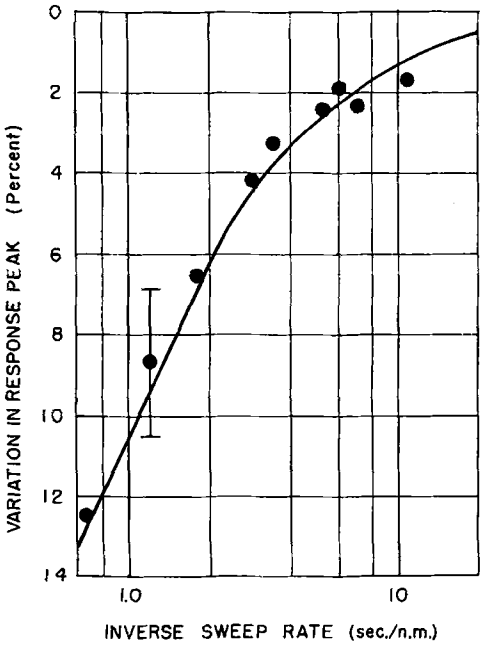

Fig. 14. Comparison of spectrally resolved photodepopulation response peak position at various sweep rates (solid circles) with the calculated model response (solid line). Sample number 1 data were used in this comparison.

As described above, the photocurrent response in the slow sweep rate limit approached the actual trapping level distribution $\rho''(\lambda)$. In Fig. 15, a slow sweep rate spectrally resolved photodepopulation response curve, converted to energy units and normalized to the photon density in the oxide film, is exhibited. The solid curve represents the gaussian function best fit to the experimental data, determined by a least squares minimization technique. The best fit curve was peaked at 2·18 eV, and had a full width of 0·55 eV. When corrected to zero sweep rate (Fig. 14), is yielded $\epsilon_T = 2{\cdot}13$ eV and $\delta = 0{\cdot}24$ eV (refer to Fig. 13).

The experimental points indicated in Fig. 15

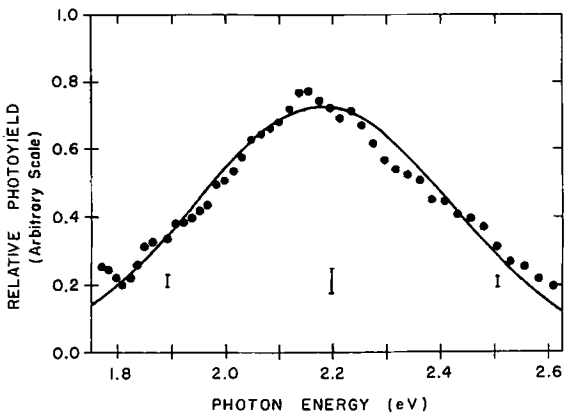

Fig. 15. Spectrally resolved photodepopulation response normalized to light intensity in the oxide (see Appendix). Data from sample number 1 at monochromator sweep rate 0·3 nm/sec. are indicated as solid circles. The solid line represents a gaussian function best fit to these data points.

and those exhibited in Fig. 2 of the Thomas and Feigl communication [33] were both computed from the same data (Fig. 5). The data in Fig. 15, however, are normalized to the photon-density in the oxide film, rather than the photon density incident on the MOS electrode. Details of this normalization are given in the Appendix.

(c) *Optical bleaching experiments*

In analyzing the optical bleaching experiments, and deriving the bleaching profile (Fig. 10), the assumptions of Sections 4(a) and 4(b) were used together with a modified description of the trapping level distribution in energy. The trapping levels associated with a given 'point defect' structure were again assumed continuously distributed in energy due to static (time-stable) fluctuations in local geometry. The width of this distribution was designated δ_s. The optical transitions to mobile states, producing the photoconductive response of interest, generally involve some combination of initial and final state densities with a thermal average over phonon states [42, 43]. The short lived local strains associated with phonon scattering were treated as a gaussian spreading of the initial localized state, leading to an *intrinsic* or *dynamic* width δ_d. The result of all this is a gaussian distribution (width δ_s) of gaussian 'packets' of states (width δ_d), so that in an interval $d\epsilon$ about energy ϵ there are

$$n_T\rho''(\epsilon)\,d\epsilon = n_T\left\{\int_{-\infty}^{\infty}\frac{1}{\sqrt{2\pi}\delta_s}e^{-\frac{(\epsilon'-\epsilon_T)^2}{2\delta_s^2}} \times\frac{1}{\sqrt{2\pi}\delta_d}e^{-\frac{(\epsilon'-\epsilon)^2}{2\delta_d^2}}\,d\epsilon'\right\}d\epsilon$$

trapping states per unit area. It can be shown that

$$n_T\rho''(\epsilon)\,d\epsilon = \frac{1}{\sqrt{2\pi}\delta}e^{-\frac{\bar{\epsilon}^2}{2\delta^2}}\,d\bar{\epsilon},$$

where $\bar{\epsilon} = \epsilon - \epsilon_T$

and $\delta = \sqrt{\delta_s^2 + \delta_d^2}$

was presumed to be the observed width of the trapping level distribution described in Section 3(b) (see Fig. 13). Thus, δ was presumed to be the zero sweep rate limit photocurrent response width in the spectrally resolved photocurrent experiments.

Optical bleaching was treated in the simplest approximation. For bleaching light of energy $h\nu_b$, all state packets of width δ_d with peak energies ϵ less than $\epsilon_b = h\nu_b$ were bleached completely. All state packets with peak energy greater than $h\nu_b$ were completely unaffected. The bleached photocurrent distribution (Fig. 9) was then simply the distribution of unbleached packets. This was given, in the slow sweep rate limit, by

$$R_b(\epsilon)\,d\epsilon = \frac{n_T}{\sqrt{2\pi}\delta}e^{-\frac{\epsilon^2}{2\delta^2}} \times\left\{1-\int_{-\infty}^{\epsilon_b-(d^2/\delta_d^2)\epsilon}e^{-\frac{\epsilon''^2}{2d^2}}\,d\epsilon''\right\}d\epsilon$$

$$= n_T\rho''(\epsilon)\left(1-F\left(\epsilon_b-\frac{d^2}{\delta_d^2}\epsilon\right)\right)d\epsilon$$

$$= R(\epsilon)\left(1-F\left(\epsilon_b-\frac{d^2}{\delta_d^2}\epsilon\right)\right)d\epsilon$$

where $R(\epsilon)$ was the zero sweep rate photocurrent response of Section 3(b), expressed in energy units rather than wavelength. In terms of previously defined experimental responses, $R_b(\epsilon) \propto I_{\epsilon_b}(\epsilon)$ and $R(\epsilon) \propto I_{\text{i.r.}}(\epsilon)$.

The bleaching profile is then

$$\frac{R(\epsilon) - R_b(\epsilon)}{R(\epsilon)} = F\left(\epsilon_b - \frac{d^2}{\delta_d{}^2}\epsilon\right)$$

where

$$F\left(\epsilon_b - \frac{d^2}{\delta_2{}^2}\epsilon\right) = \frac{1}{\sqrt{2\pi}} \int_{-\infty}^{x_b} e^{-x^2/2}\, dx,$$

$$x_b = \frac{1}{d}\left[\epsilon_b - \frac{d^2}{\delta_d{}^2}\epsilon\right].$$

is easily obtained from tabulated functions [44]. The characteristic width of the bleaching profile is given by $d = (1/\delta_s{}^2 + 1/\delta_d{}^2)^{-1/2}$.

The greatly simplified model used in this analysis is summarized in Fig. 16, together with the analytical results just stated. The model led to a universal bleaching profile, for a given distribution, that was characterized by a width d, independent of the bleaching energy ϵ_b. This was obviously in qualitative agreement with what was observed (Fig. 10).

A plot of the data of Fig. 10, fit to a universal bleaching function by graphical techniques, is exhibited in Fig. 17. From this data, the width d was estimated. It was then possible in principle to evaluate δ_s, the width of the static energy distribution of trapping levels, from the experimental numbers δ of Section 4(b) and d of the present section.

This data was internally consistent only to within a factor of three (δ can be estimated from the bleaching profile of Fig. 17, using $d^2/\delta_d{}^2$ and d to determine δ_s, as indicated in

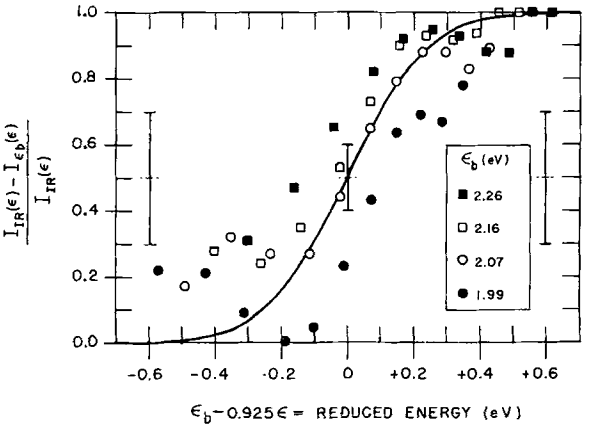

Fig. 17. Graphical best fit of experimental bleaching profiles (data points – see Fig. 10) to generalized bleaching profile (solid line).

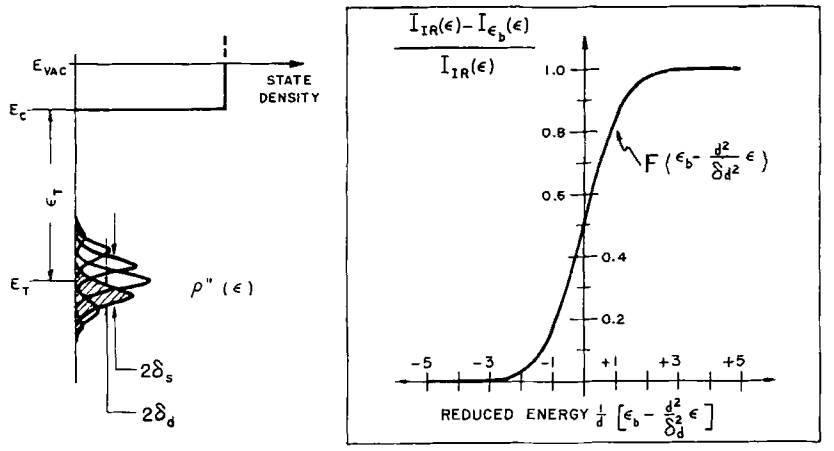

Fig. 16. Schematic representation of electronic structure model for SiO_2 used in analyzing bleaching profile data. The analysis is described in the text. The inset at right contains a representation of the generalized bleaching profile expected in bleached response experiments.

Fig. 16). However the qualitative success of the analysis provided an estimate of $\delta_d = 0{\cdot}1$–$0{\cdot}2$ eV, and $\delta_s = 0{\cdot}2$–$0{\cdot}3$ eV.

5. DISCUSSION AND CONCLUSIONS

The most important result of the present experiments was the determination of the important characteristics of the electronic structure of an electron trapping defect in silica films produced by wet oxidation of silicon. The density, geometric centroid, trap depth, and static distribution width are summarized in Table 3, and represented schematically in Fig. 18. The data of di Stefano and Eastman and Powell was used in constructing Fig. 18 [45, 46].

Table 3. Trapping state distribution characteristics in wet thermal oxide films

Trap depth	$\epsilon_T = (2{\cdot}13 \pm 0{\cdot}05)$ eV
Static distribution width	$\delta_s = (0{\cdot}25 \pm 0{\cdot}05)$ eV
Geometric centroid	$\bar{x}/L = (0{\cdot}6 \pm 0{\cdot}1)$
Trap density (Maximum observed filled trap density = lower bound).	
Sample No. 1:	$\frac{n_T}{L} = (0{\cdot}60 \pm 0{\cdot}05) \times 10^{14}\ \text{cm}^{-3}$
Sample No. 2:	$\frac{n_T}{L} > 3{\cdot}0 \times 10^{14}\ \text{cm}^{-3}$
Sample No. 3:	$\frac{n_T}{L} = (0{\cdot}4 \pm 0{\cdot}1) \times 10^{14}\ \text{cm}^{-3}$

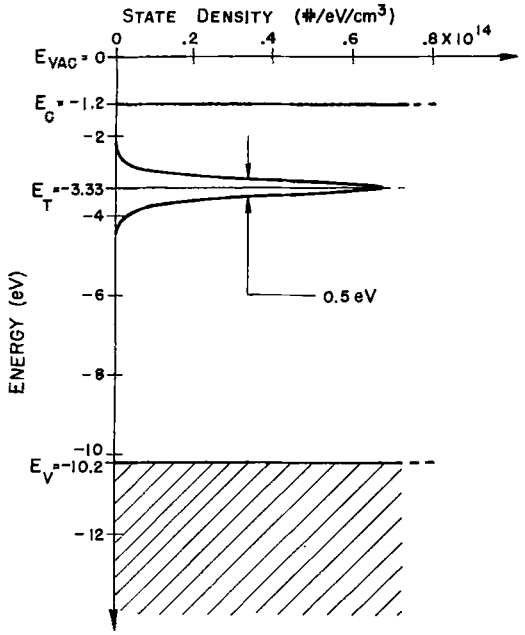

Fig. 18. Electronic structure of silicon dioxide produced by wet oxidation of silicon. E_C and E_V are taken from DiStefano and Eastman (see Refs. [45, 46]). The abcissa scale is a *lower bound* on the density of states.

An additional set of measurements had an important bearing on the fundamental qualitative conclusion set forth in Section 4. The central thesis was that there was, in silica films produced by wet oxidation of silicon, a bounded and extended distribution of electron trapping levels [38]. This electronic level distribution was presumed to be populated by trapping free carriers injected into the oxide (refer to Section 2, particularly Fig. 3(a)). It was expected that the trap distribution would fill uniformly as the number of trapped electrons increased from zero to some finite value during the photoinjection process [11].

In order to verify this assumption, and check the internal consistency of the overall logic, a series of spectrally resolved photodepopulation measurents was made for various fill conditions. These data are presented in Fig. 19. Data were recorded at constant applied voltage for both photoinjection and photodepopulation ($V = 100$ V across number 2 MOS specimen). A constant sweep rate $\beta = 0{\cdot}87$ nm/sec. was employed. The parameter in the family of curves of Fig. 19 was the fill time in the photoinjection process (refer to Section 2(a)). The data indicated that the shape of the distribution curve did not vary significantly for different fill times, and hence did not vary with the density of trapped electrons. Thus, trapping level distribution was in fact populated uniformly throughout the photoinjection, trapping, and measurement process. Specifically, the data of Fig. 19 were not consistent with trapping into an exponential band edge distribution of trapping levels [47].

The spectrally resolved data of Fig. 19 were

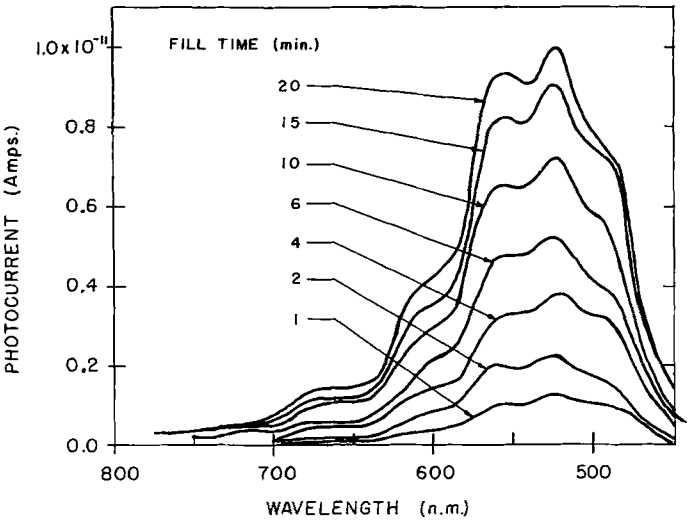

Fig. 19. Spectrally resolved photodepopulation response for various photoinjection fill times. Sample number 2, electrode area 0·18 cm², monochromator sweep rate 0·87 nm/sec.

mechanically integrated to determine the total charge released, from the trap distribution between 700 and 450 nm, as a function of trap filling time. These data, presented in Fig. 20, closely resemble William's data[11]. The latter were obtained using unfiltered visible light for photodepopulation.

It should be noted that the determination of the trap depth, together with the determination by di Stefano and Powell of the internal

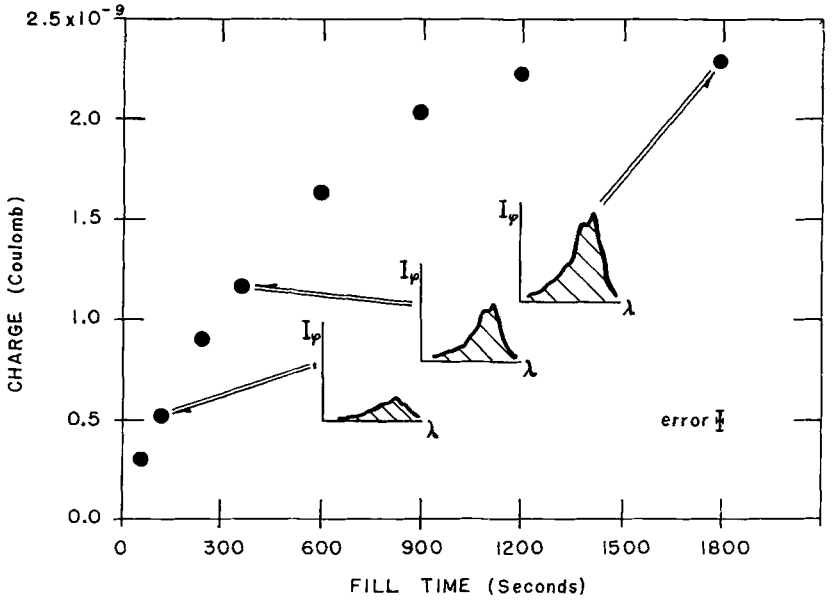

Fig. 20. Charge collected as a function of photoinjection fill time. Sample number 2, electrode area 0·18 cm². The insets (I_φ vs. λ) represent spectrally resolved responses from which data points were calculated.

photoconductive band gap of silica produced by steam oxidation of silicon, weakens Gwyn's recent association of the 2 eV electron trap in silica films with an unsatisfied oxygen bond. According to Gwyn, the unsatisfied oxygen bond should be 5·85 eV above the valence band edge, rather than 6·87 eV as indicated in Fig. 20. Optical absorption studies of bulk fused silica[48], and recent experiments by Hickmott on sputtered silica films[49], have not determined any characteristic absorption bands at 6·9 eV. The extensively studied A-absorption bands in the region 2·0–2·3 eV in quartz, bulk fused silica, and alkali glasses[48] have not been observed by Hickmott[49]. These have historically been associated directly with holes trapped on oxygen sites adjacent to Si-substituted aluminum impurities[48]. This association depends on correlation of optical absorbance with Al content and with the intensity of well-defined paramagnetic resonance absorption spectra, but it is still rather suspect[48, 50].

It should explicitly be pointed out that the present experiments did not provide any critical input to the question of the mechanism of charge injection and transport in wet grown thermal silica films. Although the present measurements were addressed to trapped electronic charge in the film, and depend on the existence of such trapping, they cannot be interpreted as supporting the interpretation of photoemission I–V characteristics in thick oxide specimens offered by Williams[11] and Goodman[12]. Specifically, the important question of the ratio of the density of trapping states to the density of filled traps after photoinjection is very much involved with the complex time dependence of the photoinjection and photodepopulation experiments. This has not been dealt with in the present paper. The assumption of filled trap distributions in the analysis of Section 3 was made for convenience only.

The existence of a large negative charge distribution in the insulator which was not released optically by photons with energy less than 4 eV was consistent with recent results reported by several groups[21, 51, 52]. Again, however, it has not been established that these fixed charges (refer to Section 4(a)) were produced by the same solid state chemical processes determined in detail by Berglund and co-workers[21, 51].

Acknowledgements—Extensive discussions with Profs. S. R. Butler and W. B. Fowler, suggestions on analysis from Profs. R. T. Folk and W. J. Van Sciver, and conversations with Drs. R. J. Powell and R. Williams are gratefully acknowledged. The experimental program benefited greatly from support of research at Lehigh via the University's Materials Liaison Program.

REFERENCES

1. GROVE A. S., *Physics and Technology of Semiconductor Devices*, John Wiley, New York (1967).
2. SZE S. M., *Physics of Semiconductor Devices*, Chapter 9, Wiley–Interscience, New York (1969); see also GOETZBERGER A. and SZE S. M., *Metal–Insulator–Semiconductor (MIS) Physics*, in *Applied Solid State Science* (Edited by R. Wolfe and C. J. Kriessman), Vol. 1, Academic Press, New York (1969).
3. KAR S. and DAHLKE W., *Appl. Phys. Lett.* **18**, 401 (1971); see also KAR S., *Interface States and Potential Barriers in Metal–SiO_2–Si Structures*, Dissertation, Lehigh University (1971), unpublished.
4. HUNTER W. R., EATON D. H. and SAH C. T., *Appl. Phys. Lett.* **17**, 211 (1970).
5. SCHLEGEL E. S., *IEEE Trans. Electron. Dev.* **ED-14**, 728 (1967); **ED-15**, 951 (1968). This is an extensive bibliography on metal-oxide-semiconductor systems, through 1967.
6. GROVE A. S., DEAL B. E., SNOW E. H. and SAH C. T., *Solid St. Electron.* **8**, 145 (1965).
7. TERMAN L. M., *Solid St. Electron.* **5**, 285 (1962).
8. LEHOVIC K. and SLOBODSKOY A., *Phys. Status Solidi* **3**, 447 (1963).
9. NICOLLIAN E. H. and GOETZBERGER A., *Bell Syst. Tech. J.* **46**, 1055 (1967).
10. KAR S., *A Critical Study of the Different Methods of Investigating Semiconductor–Insulator Interface State Properties*, M.S. Thesis, Lehigh University (1968), unpublished.
11. WILLIAMS R., *Phys. Rev.* **140**, A569 (1965).
12. GOODMAN A. M., *Phys. Rev.* **144**, 588 (1966).
13. GOODMAN A. M., *Phys. Rev.* **152**, 780 (1966).
14. GOODMAN A. M., *Phys. Rev.* **152**, 785 (1966).
15. GOODMAN A. M. and O'NEILL J., *J. appl. Phys.* **37**, 3580 (1966).
16. DEAL B. E., SNOW E. H. and MEAD C. A., *J. Phys. Chem. Solids* **27**, 1873 (1966).
17. WILLIAMS R., *J. appl. Phys.* **37**, 1491 (1966); see also WILLIAMS R., Injection by Internal Photoemission, in *Semiconductors and Semimetals*, (Edited by R. K. Willardson and A. C. Beer), Vol. 6, Academic Press, New York (1970).

18. POWELL R. J., *J. appl. Phys.* **40**, 5093 (1969).
19. POWELL R. J., *J. appl. Phys.* **41**, 2424 (1970).
20. BERGLUND C. N. and POWELL R. J., *J. appl. Phys.* **42**, 573 (1971).
21. POWELL R. J. and BERGLUND C. N., *J. appl. Phys.* **42**, 4390 (1971).
22. POWELL R. J., *IEEE Trans. Nucl. Sci.* **NS-17**, number 6, pp. 41–46 (December, 1970).
23. REVESZ A. G., *IEEE Trans. Electron. Dev.* **ED-12**, 97 (1965).
24. REVESZ A. G. and ZAININGER K. H., *RCA Rev.* **29**, 22 (1968).
25. FOWKES F. M. and BURGESS T. E., *Surface Sci.* **13**, 184 (1969). See also Ref. [30].
26. ZAININGER K. H., *Appl. Phys. Lett.* **8**, 140 (1966).
27. MITCHELL J. P., *IEEE Trans. Electron Dev.* **ED-14**, 764 (1967).
28. MITCHELL J. P. and WILSON D. K., *Bell Syst. Tech. J.* **46**, 1 (1967); see also WILSON D. K. MITCHELL J. P., CUTHBERT J. D. and LEE H. S., *Effects of Radiation on Semiconductor Materials and Devices: Final Report* (Air Force Cambridge Research Laboratory Document No. 68-0250), available from Clearinghouse for Federal Scientific and Technical Information, U.S. Dept. of Commerce.
29. GWYN C. W., *J. appl. Phys.* **40**, 4886 (1969).
30. FOWKES F. M. and BURGESS T. E., *Silicon Surface Charge Control by Interactions between Impurity Electron-Donors, Water and E_1 Centers in SiO_2*, Abstract No. 112, Electrochemical Society Meeting (4–9 May 1970, New York); also FOWKES F. M. and BURGESS T. E., *Interfacial and Bulk Interactions of E_1' Centers, Sodium and Water in Thin Layers of SiO_2 on Silicon*, preliminary manuscript.
31. DEAL B. E., SKLAR M., GROVE A. S. and SNOW E. H., *J. electrochem. Soc.* **114**, 266 (1967).
32. SNOW E. H., GROVE A. S., DEAL B. E. and SAH C. T., *J. appl. Phys.* **36**, 1664 (1965).
33. THOMAS J. H. and FEIGL F. J., *Solid State Commun.* **8**, 1669 (1970).
34. THOMAS J. H., III, *A Photoemission Study of Electron Trapping Centers in Thermally grown Silicon Dioxide on Silicon*, Dissertation, Lehigh University (1970), unpublished. Detailed descriptions of experimental and analytical techniques are given in this dissertation.
35. MOTT N. F. and GURNEY R. W., *Electronic Processes in Ionic Crystals*, 2nd edition, Oxford University Press, London (1950).
36. BUBE R. H., *Photoconductivity of Solids*, Wiley, New York (1960); see especially Chapter 9.
37. ROSE A., *Concepts in Photoconductivity and Allied Problems*, Wiley, New York (1963).
38. LAMPERT M. and MARK P., *Current Injection in Solids*, Academic Press, New York (1970).
39. PRIMAK W. and BOHMANN M., Radiation Damage, in *Progress in Ceramic Science* (Edited by J. E. Burke), Vol. 2, Pergamon Press, New York (1962).
40. BUBE R. H., *Photoconductivity of Solids*, p. 275 Wiley, New York (1960).
41. PORTIS A. M., *Phys. Rev.* **91**, 1071 (1953).
42. FOWLER W. B., editor, *Physics of Color Centers*, Academic Press, New York (1968). In particular, FOWLER W. B., *Electronic States and Optical Transitions of Color Centers*, Chapter 2, p. 70, and HENRY C. H. and SLICHTER C. P., *Moments and Degeneracy in Optical Spectra*, Chapter 6.
43. BASSANI G. F., Band Structure and Inter-band Transitions, in *The Optical Properties of Solids*, (Edited by J. Tauc), Academic Press, New York (1966).
44. ABRAMOWITZ M. and STEGUN I. A., *Handbook of Mathematical Functions: National Bureau of Standards Applied Mathematics Series 55* (Superintendent of Documents, U.S. Government Printing Office, Washington, D.C., 1964): refer to the normal probability function (Section 26.2 and Table 26.1) and error function (Section 7).
45. DiSTEFANO T. H. and EASTMAN D. E., *Bull. Am. Phys. Soc. II* **16**, 373 (1971); DiSTEFANO T. H., private communication.
46. POWELL R. J. and DERBENWICK G., *IEEE Trans. Nucl. Sci.* **NS-18**, number 6, pp. 99–105 (December, 1971).
47. LAMPERT M. and MARK P., *Current Injection in Solids*, Sections 2.8 and 4.7.1, Academic Press, New York, (1970).
48. LELL E., KREIDL N. and HENSLER J., Radiation Effects in Quartz, Silica and Glasses, in *Progress in Ceramic Science* (Edited by J. Burke), Vol. 4, Pergamon Press, New York (1966).
49. HICKMOTT T. W., *J. appl. Phys.* **42**, 2543 (1971); see also KORZO V. F., KIREEV P. S. and LYASHCHENKO G. A., *Soviet Phys.-Semicond.* **2**, 1545 (1969). This last study indicates that the 2·1 eV electron trapping center exists in silica films produced by techniques other than thermal oxidation of silicon.
50. SCHNADT R. and SCHNEIDER J., *Phys. kondens. Mater.* **11**, 19 (1970).
51. NICOLLIAN E. H., BERGLUND C. N., SCHMIDT P. F. and ANDREWS J. M., *J. appl. Phys.* **42**, 5654 (1971).
52. VISWANATHAN C. R. and OGURA SEIKI, *Proc. IEEE* **57**, 1552 (1969) also report observation of large internal charge densities in silicon dioxide layers on silicon. More detailed discussion is given in OGURA S., *Solid Interface Studies by Photoelectric Technique* (Dissertation, University of California, Los Angeles (1969), unpublished.
53. HEAVENS O. S., *Optical Properties of Thin Solid Films*, Butterworths, London and Academic Press, New York (1955).
54. PHILIPP H. R. and TAFT E. A., *Phys. Rev.* **120**, 37 (1960).
55. UNSÖLD A., *Physik der Sternatmosphären*, Springer-Verlag, Berlin, (1955), Zweite Auflage, IX Kapitel.

APPENDIX: OPTICAL MODEL OF M-O-S SPECIMENS

Light intensity variations in the oxide, due to the optical response of the MOS structure, were calculated to produce the normalized photoyield for spectrally resolved

data [refer to Section 4(b), especially Fig. 15]. The model used to calculate this optical response will now be discussed in some detail.

The optical response, which includes the effects of the thin gold electrode, the silicon substrate optical properties, and the pass band of the monochromator, has been calculated using a two-layer dielectric structure, as shown in Fig. 21. For normally incident light, of wavelength λ, on a two-layer dielectric structure, the reflected intensity is [53]:

$$R(\lambda) = \frac{r_1^2 + r_2^2 + 2r_1 r_2 \cos 2\delta_1}{1 + r_1^2 r_2^2 + 2r_1 r_2 \cos 2\delta_1}. \qquad (A.1)$$

Here, $\delta_1 = 2\pi n_1 L/\lambda$, L is the oxide thickness as shown in Fig. 21, and r_1 and r_2 are the Fresnel coefficients at the Au–SiO_2–Si interfaces, respectively. The Fresnel coefficients for normal incidence are

$$r_1 = \frac{n_0 - n_1}{n_0 + n_1} \quad \text{and} \quad r_2 = \frac{n_1 - n_2}{n_1 + n_2}, \qquad (A.2)$$

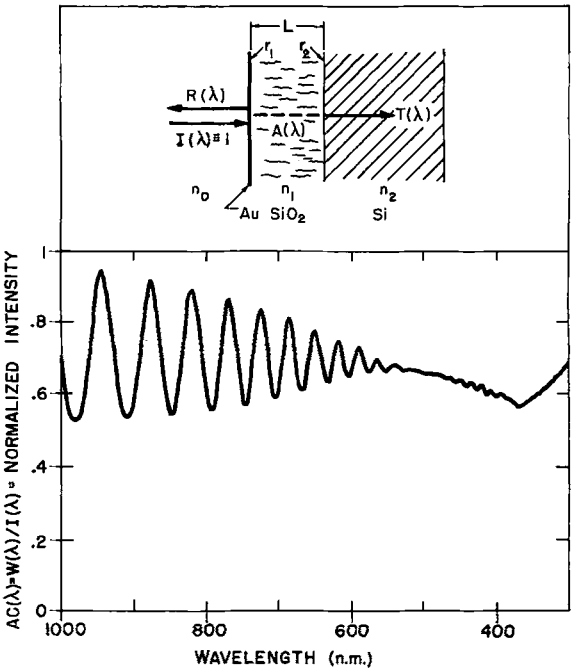

Fig. 21. Schematic representation of model employed in calculating optical intensity in the oxide layer (upper diagram). The lower diagram is the normalized intensity, including monochromator pass band effects, calculated from this model.

where n_0, n_1 and n_2 are refractive indices for air, silica, and silicon. The effect of the thin gold electrode was included by increasing the reflectivity of the air–oxide interface, r_1. This value was determined from data in Heavens [53]. r_2 was calculated using the Taft and Phillips data for silicon [54]. The calculated values for r_1 and r_2 were then substituted into equation (A.1). The intensity of light in the oxide layer, $A(\lambda)$ was found by

$$A(\lambda) = 1 - R(\lambda) \qquad (A.3)$$

since the oxide is assumed to be nonabsorbing. Assuming the oxide thickness is 4·0 μm, $A(\lambda)$ becomes (for λ in micrometers), in equation (A.4),

$$A(\lambda) = \frac{k_1}{k_2 + \cos(24\pi/\lambda)} \qquad (A.4)$$

$$k_1 \approx k_2[1 + r_1^2 r_2^2 - r_1^2 - r_2^2] \quad \text{and} \quad k_2 \approx \frac{1}{2r_1 r_2}.$$

A further consideration was necessary in describing the wavelength dependence of the undulation amplitude as observed in actual photocurrent response measurements (refer to Fig. 5). Data indicate that the magnitude of the undulations decreased with decreasing wavelength. This effect was related to the finite pass band of the monochromator. Since the separation of undulation maxima varied inversely with λ (equation (A.4)), the effect of averaging the undulation amplitude in the monochromator pass band became more pronounced as the wavelength was decreased. Slit width effects were included by convolving a function describing the monochromator pass band shape with the intensity function in the oxide, $A(\lambda)$ [55]. The spectral distribution of the monochromator is triangular in shape with the apex position corresponding to the monochromator dial setting. If the slit function, $S(\lambda)$, is convolved with the intensity in the oxide, the resultant convolved intensity in the oxide is given by

$$AC(\lambda) = \int_{-\infty}^{\infty} d\lambda_0 S(\lambda_0 - \lambda) \frac{k_1}{k_2 + \cos(24\pi/\lambda_0)} \qquad (A.5)$$

where λ_0 is an integration variable. The results of a numerical simulation on this model are shown in Fig. 21 for $r_1 = 0{\cdot}45$.

The convolved response, $AC(\lambda)$, thus obtained was used with the Xenon lamp spectrum, $I(\lambda)$, to compute the normalized photoyield of Fig. 15. This is to be compared with Fig. 2 of the Thomas–Feigl communication [33], which was normalized to the Xenon lamp spectrum $I(\lambda)$. The intereference undulations have been adequately described by the straightforward model of Fig. 21, using a photoyield normalization of the form $(hc/\lambda)(I_\varphi/W(\lambda))$. I_φ is the photocurrent measured at λ (Fig. 5) and $W(\lambda) = I(\lambda)AC(\lambda)$, as indicated in Fig. 21.